*(IJIRSE)International Journal of Research in Science and Engineering*
*ISSN (Online) 2347-3207*

# Micro structural parameters of Silver Nano particles using whole pattern fitting technique

**Mahesh S S[1], Prashanth K S[2], Ananda S[3], Nanda Prakash[4], R.Somashekar[5]**

Professor, Department of Physics, Acharya Institute of Technology, Bangalore 560 090,India [1]

Assistant Professor, Department of Physics, New Horizon College of Engineering, Bangalore, India[2]

Department of Physics, Sapthagiri College of Engineering, Bangalore 560 090, India[3]

Research Scholar, Department of Studies in Physics, University of Mysore, Manasagangotri [4]

Professor, Department of Studies in Physics, University of Mysore, Manasagangotri,
Mysore 570 006, Karnataka, India[5]

*Abstract*- **Silver Nano particles are synthesized by Conventional method of biosynthesis of silver nano particles using extract of Parthenium hysterophorus. The synthesized Nano particles were subjected to XRD and SEM analysis for the characterization process for estimating the size of crystalline particle and figure out the morphology. The as-prepared powders are all nano-sized ( nm) and the same is confirmed by broadening of the X-ray diffraction peaks and Scanning electron microscopy. XRD results show that Crystallite area decreases with increasing concentration. The crystallite size (<N>), lattice strain (g in %), stacking faults ($\alpha^d$) and twin faults (β) determined by whole powder pattern fitting technique, developed by us.We have studied the microcrystalline parameters from XRD. Activation energy has been computed for these systems.**

**Key Words: Stacking and Twin faults, Micro structural parameters, WAXS,**

## INTRODUCTION

The systems being designed and produced at incredibly small scale of atoms and molecules. This field of science has made its place in production of nanomaterials which are regarded as ‘ first generation’ products, that includes nanoparticles, nanocrystals, nanobiomotors, nanowires, quantum dots etc. The worldwide emergence of nanoscale sciences and engineering was marked by the announcement of the National Nanotechnology Initiative (NNI) in Jan 2000 [1]. Nanomaterials are the leading edge because of their unique properties which has enabled the technology to acquire the superiority in the applied fields and made it indispensible in areas of human activity [2]. A decade ago,nanoparticles were studies because of their size-dependent physical and chemical properties[3]. Now they have entered a commercial exploration period [4,5] With the development, nanomaterial level is now the most advanced in both scientific knowledge and commercial applications. Nanoparticles are engineered structures with

at least one dimension of 100 namometers or less. These novel materials are increasingly used for commercial products, including developing new designs for medicinal applications[6].

Metal nanoparticals such as gold and silver have been recognized to be important in the fields of chemistry, physics and biology. These particles are being processed for various purposes because of their remarkable properties such as conductivity, biocompatibility, optical, photothermal, magnetic, catalytic properties and also antimicrobial activity. The size and size distribution of the particles is extremely a critical condition to be considered. Other physiochemical factors which are also important are shape, morphology, charge, area, reactivity and chemical surroundings [7-13].Synthesis of Ag nanoparticles can be achieved by chemical routes[14], or by means like sol-process, sol-gel process, pyrolysis[15], chemical vapour deposition, gas condensation, co- condensation[16],thermal decomposition, radiation assisted, microwave radiation assisted process or by bio-based protocols using either microbial or plant extract. In the process of synthesis, aqueous solution of silver nitrate is reduced to silver nanoparticles by the reducing agent used in the corresponding method adopted. Some of the chemicals used by researches are citric acid [17], trisodium citrate [18], borohyride[19], DAPHP[7], ethanol[20] for the purpose of reduction. Although chemical method is the simple one [14] the use of environmentally benign materials like certain plant extracts, bacteria or fungi for the synthesis offers numerous benefits of eco-friendliness, cost-effectiveness and compatibility. And since chemical synthesis would often lead to presence of remains of toxic chemical species absorbed on the surface biological method would be preferred. Different strains of microorganisms used are Fusarium oxyspores, Bascillus subtillis[21], yet this still remains tedious due to the fact that microbial source always need to be handled with lot of care due to high chances of contamination. With all this, the development of green synthesis is now evolving into an important branch where plant extract is used. Bio-inspired synthesis offers several other advantages like elimination of high pressure and energy as well. We have used Parthenium hysterophorus. This plant is an obnoxious weed which is popularly called as Congress weed. This was introduced in India in 1956 and spread over most part of the country [22]. It is known for causing skin itching just by touch for which its considered regardless. We have worked to get the best out of this undesirable weed, for synthesis of silver nanoparticles. On reduction silver ions present in aqueous solution of silver complex in Parthenium extract can be demonstrated with the change in colour which is due to formation of nanoparticles.

# MATERIALS AND METHODS

## A.*Prepation of plant extract*

25g of fresh Parthenium hysterophorus leaves collected from campus of PESIT were thoroughly washed, cut into fine pieces and boiled in 100ml millipore water for 10 minute broth was filtered using Whatman's filter paper and filter was used as reducing agent to reduce silver.

## B.*Synthesis of silver nanoparticles*

*Conventional method of biosynthesis of silver nanoparticles using extract of Parthenium hysterophorus*

1mM silver nitrate solution was prepared by dissolving 0.16g of AgNO3 n 1000ml millipore water. Extract added to silver nitrate in the ratio 1:5 and the mixture is incubated under dark conditions at room temperature for 5 days facilitating the formation of silver nanoparticles.

*Rapid method of biosynthesis of silver nanoparticles using extract of Parthenium hysterophorus*

Extract treated with 1mM AgNO3 in the ratio 1:5, the reaction mixture was subjected to several short burst of microwave irradiation in a cyclic mode. A cycle constituting 15sec exposure to microwave radiation and 20sec of non-exposure to prevent over heating as well as aggregation of metals. The reaction mixture was monitored by sampling of aliquot(1ml) of solution after 5,7,9,12 and 15 cycles. Suspension is centrifuged at a speed of 1000rpm for 30 min and pellet was collected. Wash the pellet thoroughly and dried in a hot air oven.

## C.*UV-Vis Spectrophotometric analysis*

Change in color of reaction mixture from yellow to reddish brown is an indication of silver nanoparticle formation. The bio reduction of silver ions is monitored using UV Vis 1601 Shimadzu Spectrophotometer. 1ml of sample aliquot diluted with millipore water and subjected to spectrophotometry as function of reaction time with millipore water as reference.

## *D.The X-ray diffraction pattern*

X-ray diffraction pattern of silver Nano particles were recorded on Rigaku Miniflex II Diffractometer with Ni filtered, $CuK_{\alpha}$ radiation of wavelength 1.542 Å, and a graphite monochromator. The scattered beam from the sample was focused on to a detector. The specifications used for the recording were 30 kV and 15 mA. The silver Nano particles were

scanned in the 2θ range of $6^0$ to $60^0$ with a scanning step of $0.02^0$. The X-ray scattering measurements were performed at the WAXS/SAXS beam line of the LNLS (Laboratorio Nacional de Luz Sincroton-Campinas, Brazil), by using monochromatic beam of wavelength 1.7433 Å. The scattering intensity was registered using a one dimensional position-sensitive gas detector for a sample-detector distance of 1641.5 mm. The scan range (2θ) was $10^0$ to $50^0$. WAXS curves were obtained from the WAXS images by band integration tool supplied by X-ray 1.0 software, produced by University Mons Hainaut.

## II.THEORY

### *A. X-ray diffraction data analysis*

The contribution of crystallite size, lattice strain and stacking faults to a Bragg reflection profile can be written as [28],

$$I_{hkl}(s_{hkl}) = \int_{-\infty}^{\infty} T^{IP}(nd) e^{[2\pi i\zeta(nd)]} e^{[2\pi i\phi(nd)]} e^{[2\pi i nd s_{hkl}]} d(nd) \qquad (1)$$

where $I_{hkl}(s_{hkl})$ is the intensity of a profile in the direction joining the origin to the center of the reflection, $T^{IP}$ is the Fourier transform of instrument profile, $e^{[2\pi i\zeta(nd)]}$ is the average phase factor due to lattice distortion(ζ) and $e^{[2\pi i\varphi(nd)]}$ is due to crystallite size / stacking faults(φ). L = nd (with $d=d_{hkl}$) is the column length. Equation (1) can be written in the form of Fourier series as,

$$I_{hkl}(s_{hkl}) = \sum_{n=-\infty}^{\infty} A_{hkl}(n) \cos\{2\pi n d_{hkl}(s-s_0)\} \qquad (2)$$

where $A_{hkl}(n)$ are corrected Fourier coefficients with Fourier coefficients of instrumental profile function $T^{IP}(nd)$, s is $\sin\theta/\lambda$ and $s_0$ is the value of s at the peak of the reflection. Here afterwards, we refer to crystallite size in terms of the average number of unit cells counted in a direction perpendicular to the Bragg plane (hkl) with a notation <N>, and the crystallite size in Å is given by $D_{hkl} = \langle N \rangle d_{hkl}$ ($d_{hkl}$ is the perpendicular spacing of the (hkl) planes from their origin). These Fourier coefficients $A_{hkl}(n)$ are functions of the size of the crystallite, the disorder of the lattice and stacking faults coefficients, i.e.

$$A_{hkl}(n) = A^s_{hkl}(n).A^d_{hkl}(n).A^F_{hkl}(n) \qquad (3)$$

Fourier analysis of a Bragg reflection profile must always be performed [28] over the complete cycle of the fundamental form $d(s-s_o)$ = -1/2 to +1/2, which is rarely possible experimentally.

We do this analysis with the available truncated range by introducing truncated correction [29]. For a paracrystalline material, with Gaussian strain distribution, $A^d_{hkl}(n)$ turns out to be[28,30-31],

$$A^d_{hkl}(n) = \exp(-2\pi^2 n^2 m g^2) \qquad (4)$$

where m is the order of the reflection and g = (Δd/d) is the lattice strain. Normally one also defines mean square strain $<\varepsilon^2>$ that is given by $g^2/n$. This mean square strain is dependent on n (or column length L = nd), where as g is not. With exponential distribution function for column length, we have,

$$A^S_{hkl}(n) = \begin{cases} A(0)\left(1 - n/\langle N\rangle\right), & ;\text{if } n < p \\ A(0)\left\{\exp\left[-\alpha\ (n-p)\right]\right\}/(\alpha\ N) & ;\text{if } n \geq p \end{cases} \qquad (5)$$

In the above equation α = 1/(N-p), refers to the width of the distribution and p is the smallest number of unit cells in a column.

Warren [28] has given an integral analysis for deformation faults and twin faults in various crystal systems. According to this paper, the shift, broadening and asymmetry of the profile are proportional to these fault densities. The sequence of stacking layers is usually denoted by A, B and C. The unfaulted sequence is ABCABC or CBACBA. A stacking fault can be represented by AB<u>CB</u>CABC. A twin fault sequence is ABCAB<u>CBA</u>CBA. The chance of finding a stacking fault between any two adjacent layers causing a Bragg reflection and is denoted by $\alpha^d$. Normally $\alpha^d$ is expressed in percentage and the average number of Bragg planes between stacking faults is given by $1/\alpha^d$. The twin fault probability βis defined as the chance of finding a twin fault between any two adjacent (hkl) layers and the average number of (hkl) layers between twin faults is 1/β. With these aspects, Veltrop [32] has obtained an equation for Fourier coefficients $A^F_{hkl}(n)$ in terms of the deformation faults ($\alpha^d$) and twin faults (β) probabilities as

$$A^F_{hkl}(n) = [1 - 3\alpha^d - 2\beta + 3(\alpha^d)^2]^{\left|(1/2)nd_{hkl}s(L_0/h_0^2)\sigma_{L_0}\right|} \qquad (6)$$

where$\alpha^d$and β are, respectively the deformation and twin fault probabilities, $L_0$=h+k+l, $h^2_0$=$h^2$+$k^2$+$l^2$ and $\sigma_{L_0}$ is the volume of crystallite with specified $L_0$. We have assumed $\sigma_{L_0}$ to be positive for all reflections (for $L_0$=3N+1 and N = 0, ±1, ±2, . . . ) studied here. The whole powder pattern of samples were simulated using individual Bragg reflections represented by the above equations using

$$I(s) = \sum_{hkl} (\omega_{hkl} I_{hkl} - BG) \quad (7)$$

where $\omega_{hkl}$ are the appropriate weight functions for the (hkl) Bragg reflection. Here s takes the whole range ($2\theta \approx 6^0$ to $60^0$) of X-ray diffraction recording of the sample. BG is an error parameter introduced to correct the background estimations.

## III RESULTS AND DISCUSSION

### *A. SEM and TEM analysis of silver nanoparticles*

Powder extracted was subjected to electron microscopy studies to determine the morphology and size of the synthesized silver nanoparticles. SEM data helped us to figure out the morphology wherein TEM gives the size shown in **Figure 1 and Figure 2.**

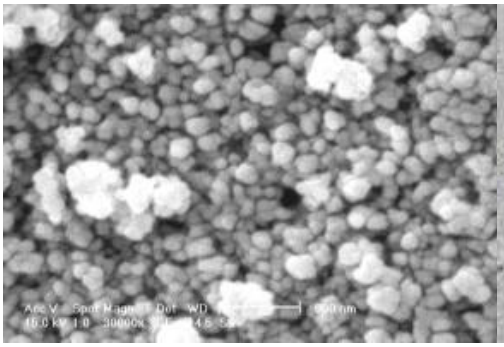

Fig.1. SEM micrograph

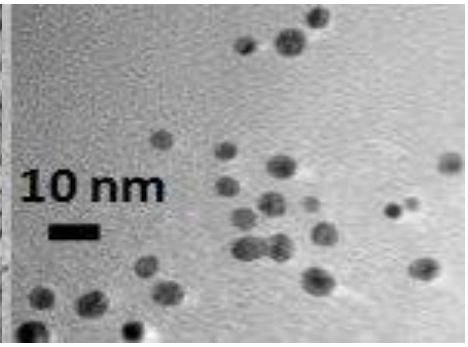


Fig.2. TEM micrograph

*Parthenium hysterophorus* leaf extract appears green in color shown **Figure 3**. This extract treated with 1mM and 2mM $AgNO_3$ and incubated at room temperature for 7 days placed, the color of the change in the color of in the suspension to reddish brown is the primary indication of the formation of silver nanoparticles. Change in color which is due to the excitation of Suface Plasmon Resonance (SPR).In metal nanoparticles such as silver, the conduction band and the valence band lie very close to each other in which electrons move freely. These free electrons give rise to SPR absorption band occurring due to the collective oscillation of electrons of silver nanoparticles in resonance with light wave. Classically, the electric field of an incoming wave induces a polarization of the electrons with respect to much heavier ionic core of silver nanoparticles. As a result a net charge difference occurs which in turn acts as a restoring force. This creates a dipolar oscillation of all the electrons with the same phase. When the frequency of the electromagnetic field becomes resonant with the coherent electron motion, a strong absorption takes place, which is the origin of the observed colour [35]**Figure 4.**

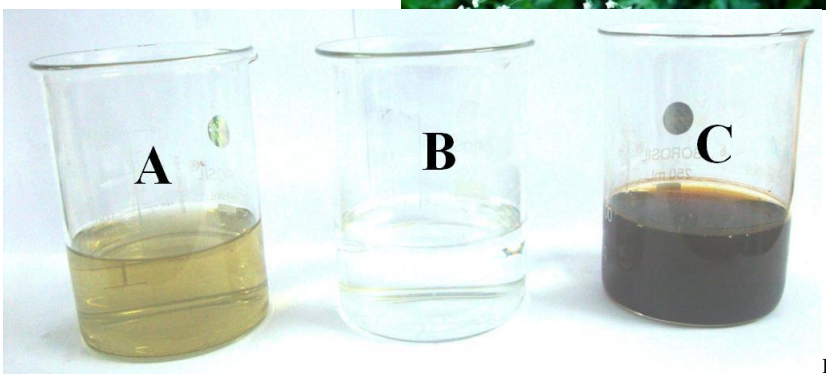


Fig 3.Parthenium hysterophorus plant. Fig.4. A. Picture showing the leaf extract of *Parthenium hysterophorus*, Fig.4.B. Picture showing 1mM $AgNO_3$ solution without the leaf extract, Fig.4C. Picture showing the resulting mixture of plant extract and silver nitrate (1:5) 5 days of incubation.

Rapid biosynthesis method, where in the mixture is irradiated with 5,7,9,12 and 15 cycles, **Figure 5**. Shows the gradient in the color formation from yellow to reddish brown respectively. The reduction of silver to nanoparticles increasingly proceeds with the increase number of cycles in other words increase in time of exposure to radiation.

UV-Vis absorbance spectra of silver nanoparticles biosynthesized conventionally by treating 1ml aqueous AgNO3 solution with leaf extract of *Parthenium hysterophorus* is shown in **Figure 6**. The wavelength, $\lambda_{max}$ is obtained at 426 nm with absorbance value 2.731.The sharp peak and the Surface Plasmon Resonance band in the silver nanoparticles is shown in **Figure 7** for $5^{th}$,$7^{th}$,$9^{th}$,12 and $15^{th}$ cycles also remain close to 420nm suggests that particles are monodispersed and distributed with no evidence of aggregation.

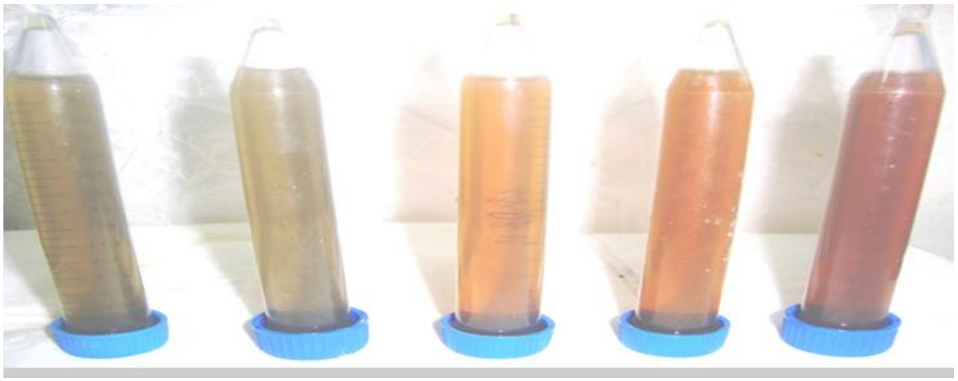

Fig.5. Picture showing the samples after rapid biosynthesis of silver nanoparticles using *Parthenium hysterophorus* leaf extract at the end of 5th cycle, 7th cycle, 9th cycle, 12th cycle and 15th cycle respectively.

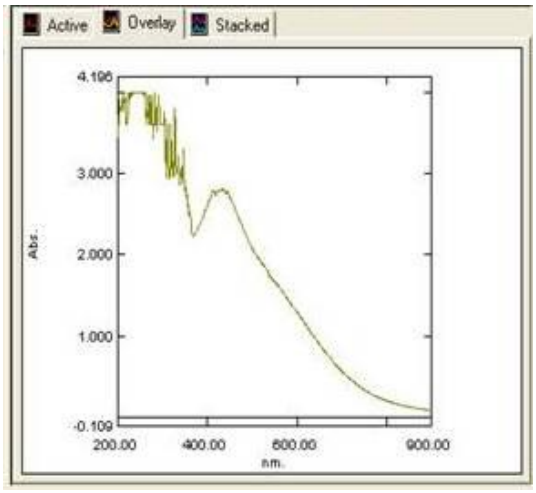


Fig 6. UV-Vis absorbance spectra of silver nanoparticles Conventionally

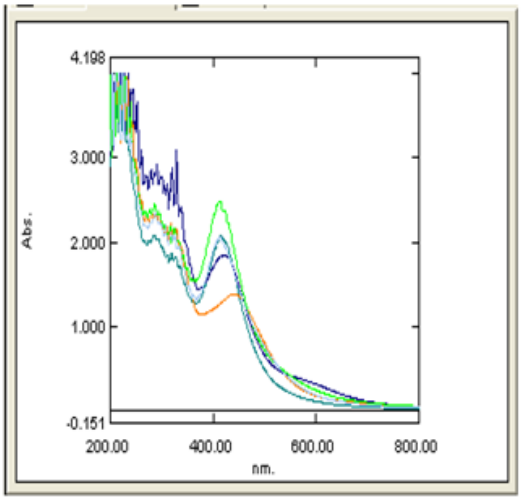


Fig.7 UV-Vis absorption spectra of silver naoparticles derived using rapid biosynthesis

One major advantage of this rapid biosynthesis method is time required for the formation of nanoparticles. Conventional incubation method takes 7days where in with the help of irradiation, silver nanoparticles can be synthesized within few sec. The other advantages of using microwave radiation are that it provides uniform heating around the nanoparticles and can assist the digestive ripening of such particles without aggregation. The microwave radiation heats up a material through its dielectric loss, which converts the radiation energy into thermal energy. Rapid microwave heating also provides uniform nucleation and growth conditions, leading to homogeneous nanomaterials with smaller sizes. Power dissipation is fairly uniform throughout with “deep” inside-out heating of the polar solvents, which leads to a better crystallinity [33].

XRD patterns obtained for silver nanoparticles synthesized by rapid method using extract of Parthenium hysterophorus at $12^{th}$ cycle marked (111) indexed based had the cubic structure. The XRD pattern of 1mM Ag ions is known to display peak at 2θ= 38.1,44.3,64.4,77.4,81.5 and 2mM Ag ions is known to display peak at 2θ=27.2,31.6,45.6,54.1,56.8.

Average particle size can be estimated using Debye-Scherrer formula given by

$$\mathbf{D = 0.9\ \lambda\ /\ W\ Cos\ \theta}$$

Where D is the particle size

λ is the wavelength of X ray= 0.1541nm

W is Full Width at Half Maximum (FWHM)

Calculation

D = (0.9 * 0.1541)/ 0.0157 *Cos (19)

= 9.3 **nm**

Hence theoretical value of the particle size is found to be 9.3nm.

A typical TEM and SEM micrographs are shown in the **Figure 1**&**Figure 2** respectively of silver nanoaprticles obtained by the synthesis of *Parthenium hysterophorus* leaf extract. With the help of these micrographs, the average particles size of silver nanoparticles is around 10nm and is cubical in shape. TEM analysis helps us to determine the size of the particles this is due to the fact that during transmission electron microscopy the electrons penetrate through the particle and the beam of electron are analyzed.SEM ananlysis helps us to determine the morphology of the particle since the electrons from the surface are reflected and the beam is of these reflected electrons are scanned. The size value is in accordance with the theoretical value of size of the silver nanoparticles as per XRD analysis.In addition to this the micro structural parameters were refined for individual profiles of X-ray recordings in each of the sample and the computed values of crystallite size <N>, lattice strain (g in %), stacking fault probability and twin fault probability are given in Table 1 for Silver nano particles using exponential distribution function.

We observe that the average crystallite area in 1mM Ag nanoparticlesis 43919 $Å^2$which decreases in 2mM Ag nanoparticles to 29313 $Å^2$. **Figure 8**shows simulated and experimental profiles for Silver Nano particles obtained with exponential column length distribution

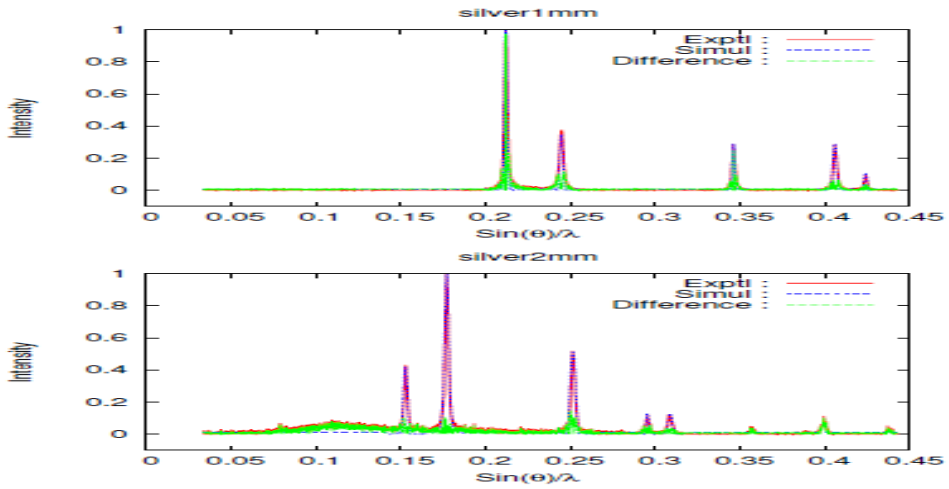


**Figure 8:** Simulated and experimental profiles for Silver Nano particles obtained with Exponential column length distribution

The standard deviations in all the cases for the micro structural parameters are given in Table 1 as Δ. This Δ represents the statistical percentage of deviation of the parameters. The agreement between simulated and experimental intensity of the individual profiles in each of the samples are less than 10% of the mean value. With these parameters given in Table 2 and Table 3 as an input, we have further refined these parameters against the whole pattern ($2\theta \approx 6^0$ to $60^0$) recorded from the samples by taking summation which extends over the whole pattern [equation (7)]. We have observed small but significant changes in these parameters with the set convergence of 1%. These changes are also given in Table 1. The goodness of the fit between simulated and experimental profiles for the samples were given in Figure 8.

**TABLE 1: Micro structural parameters and stacking faults for Silver 1 mM and Silver 2mM using exponential distribution function**

| Samples | 2θ | N | d (Å) | D (Å) | g (%) | $\alpha^d$ ($10^{-4}$) | β ($10^{-4}$) | Delta ($10^{-4}$) | Crystallite area (Å$^2$) |
|---|---|---|---|---|---|---|---|---|---|
| **Silver 1mM** | 38.1 | 88.55 | 2.36 | 208.9 | 0 | 1.42 | 0.51 | 3.97 | 43919 |
| | 44.3 | 100.5 | 2.04 | 205.0 | 0 | 1.18 | 1.51 | | |
| | 64.4 | 170.5 | 1.44 | 245.5 | 0 | 1.22 | 3.92 | | |
| | 77.4 | 145.5 | 1.23 | 178.9 | 0 | 0.88 | 0.13 | | |
| | 81.5 | 190.9 | 1.17 | 223.3 | 0 | 0.20 | 0.27 | | |
| **Silver 2mM** | 27.2 | 49.74 | 3.27 | 162.6 | 0 | 0.45 | 0.59 | 3.73 | 29313 |
| | 31.6 | 43.49 | 2.82 | 122.6 | 0 | 0.09 | 0.61 | | |
| | 45.6 | 63.80 | 1.98 | 126.3 | 0 | 0.36 | 1.12 | | |
| | 54.1 | 141.5 | 1.69 | 239.1 | 2 | 0.08 | 0.16 | | |
| | 56.8 | 94.57 | 1.61 | 152.2 | 0 | 0.69 | 0.55 | | |

The observed variation in the micro structural parameters given in Table 1 is due to a two-fold refinement. First we have carried out the line profile analysis of the extracted profiles from overlapping regions, which is a standard procedure to compute the micro structural parameters. Secondly, the range of overlapping regions determines the extent of broadening of the reflections. In fact, the broadening may decrease if the reflections are closer together and hence results in an increase in the crystallite size values. A closer look at the results in Table 1 and also the whole pattern indicates such a problem. It is worth noting that none of other parameters, such as lattice strain and stacking fault probability, varied much during the refinement against the whole pattern data of the samples. To check the reliability of the computed deformation and twin faults, we have used a simple approximate method suggested by Warren [28] and the expression for the twin fault is given by,

$$(2\theta^0_{CG} - 2\theta^0_{PM})_{hkl} = -14.6X_{hkl} \tan\theta \text{ x } \beta \qquad (8)$$

where $2\theta^0_{CG}$ is the center of gravity of the Bragg reflection profile and $2\theta^0_{PM}$ is the peak maxima, $\beta$ is the twin fault and $X_{hkl}$ is the constant value, which we have taken to be 0.23. For all the samples we have computed the average twin fault probabilities are comparable to the values obtained by incorporating an appropriate expression in the Fourier coefficients. From this we would like to emphasize that these values are reliable and do represent the twin faults present in the sample in a direction perpendicular to the axis of sample. In fact, $1/\beta$ represents the number of layers between two consecutive twin fault layers. We have also approximately estimated the deformation fault probability value $\alpha^d$ by making use of the following expression given by Warren [28],

$$\frac{1}{< D_S >} = \frac{1}{< D >} + [(1.5\alpha^d + \beta)/d_{hkl}]\ [\sum_b |L_0|/(u+b)h_0] \qquad (9)$$

Where $h_0 = (h^2+k^2+l^2)^{1/2}$ , u is the un broadened component, b is the broadened component and $L_0$=3N+1 reflections.. A comparison with the deformation fault probability values obtained by Fourier coefficient method (Table 1) indicates that the values are low, because there are too many layers between two successive deformation fault layers. This is due to the fact that there are pockets of crystalline like order in a matrix of amorphous regions. It is well known that the Fourier method gives a reliable set of micro structural parameters and we have shown that in addition to these values, one can also compute reliable fault probabilities.

A graphical plot of the crystallite shape ellipse was obtained by taking the crystal size value corresponding to $2\theta \approx 38.1^0$ along the X-axis and the other parameter corresponding to $2\theta \approx 81.5^0$ along the Y-axis for 1mM Ag Nanoparticles and $2\theta \approx 27.2^0$ along the X-axis and the other parameter corresponding to $2\theta \approx 56.8^0$ along the Y-axis for 2mM Ag Nano particles with are shown in **Figure 10**.These crystallite shape ellipse for the different samples the strength of the samples are normally proportional to crystalline area which is equal to ellipse area determined by micro structural parameters.It is evident that the crystallite shape ellipse area in 1mM Ag Nano particles is greater than 2mM Ag Nano particles.The stacking faults and twin faults for silver nanoparticles are found to be very smallwhich is shown in **Figure 9.**We have calculated the probability of finding a hexagonal or cubic environment in the stacking arrangement, which are the parameters used in the early works of Jagodzinski [27-28] and these values are given in the Table 1.

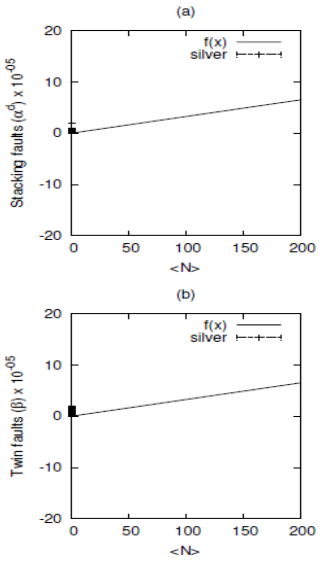


**Figure 9.**The stacking faults and twin faults for silver nanoparticles

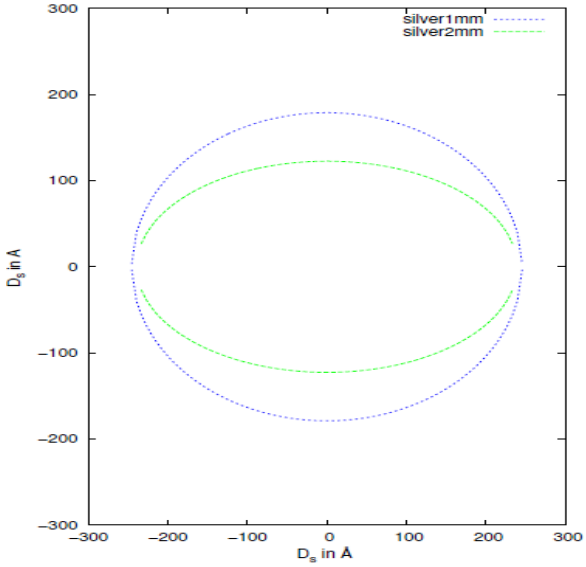


**Figure 10:** Variation of crystallite shape ellipsoid for Silver Nano particles

## IV CONCLUSION

Whole X - ray pattern fitting procedure developed by us has been used to compute micro crystalline parameters. Electron scanning micrograph study of Ag nanoparticles gives a value of the particle size in conformity with the X - ray results. The important aspect of this investigation is that 1mM Ag nanoparticles have more crystalline area than 2mM Ag silver nanoparticles studied here. The stacking faults and twin faults for silver nanoparticles are found to be very

small. The biosynthesis of silver nanoparticles by reducing Ag+ using the leaf extract of the plant *Parthenium hysterophorus* has been demonstrated. Green synthesis approach for synthesis is advantageous over chemical methods as its economical and also eco-friendly. The formation of silver nanoparticles is faster with rapid biosynthesis method compared to conventional incubation method.

## References:

1. Mihail C Roco. Current Opinion in Biotechnology 14, 337-346 (2003)
2. OV Salata. BioMed Central 2,1-6( 2004)
3. Murray CB, Kagan CR, Bawendi MG. *Annu Rev Mater Sci* 30,545-610(2000)
4. Mazzola L. *NatureBiotechnology* 21,1137-1143 (2003)
5. Paull R, Wolfe J, Hebert P, Sinkula M. *Nature Biotechnology* 21,1134-1147(2003)
6. Wilson Roa, James Xing. Nanotechnology:Public call for evidence.
7. Melissa M. Kemp, Ashavani Kumar, Shaymaa Mousa, Tae-Joon Park,Pulickel Ajayan, Natsuki Kubotera, Shaker A. Mousa, and Robert J. Linhardt. Biomacromolecules 10 (3), 589-595 (2009)
8. O'Neal, D. P. Hirsch, L. R. Halas, N. J Payne, J. D. West. J. L.Cancer Lett. (Amsterdam, Neth.) 209, 171–176 (2004)
9. Hirsch, L. R. Stafford, R. J. Bankson, J. A. Sershen, S. R. Rivera,B. Price, R. E. Hazle, J. D. Halas, N. J. West. J. L. Proc. Natl.Acad. Sci. U.S.A. 100, 13549–13554 (2003)
10. Huang, X. El-Sayed, I. H. Qian, W. El-Sayed, M. A. J. Am. Chem.Soc. 128, 2115–2120 (2006)
11. Cognet, L. Tardin, C. Boyer, D. Choquet, D. Tamarat, P. Lounis. B. roc. Natl. Acad. Sci. U.S.A. 100, 11350–11355 (2003)
12. Skirtach, A. G. Dejugnat, C. Braun, D. Susha, A. S. Rogach, A. L.Parak, W. J. Moehwald, H. Sukhorukov, G. B. Nano Lett 5,1371–1377 (2005)
13. Li, J. Wang, X. Wang, C. Chen, B. Dai, Y. Zhang, R. Song, M.Lv, G.Fu. D. ChemMedChem 2, 374–378 (2007)
14. Jun Sung Kim, Eunye Kuk, Kyeong Nam Yu, Jong-Ho Kim Sung Jin Park, Hu Jang Lee, So Hyun Kim, Young Kyung Park, Yong Ho Park, Cheol-Yong Hwang, Yong-Kwon Kim, Yoon-Sik Lee, Dae Hong Jeong, Myung-Haing Cho. Nanomedicine: Nanotechnology, Biology, and Medicine 3 (2007)
15. Asta, Judita PUISO. Material science 12,1392-1320 (2006)
16. Catauro M, Raucci MG, De Gaetano FD, Marotta A. J Mater Sci Mater Med 15(7):831 – 7 (2004)
17. Crabtree JH, Burchette RJ, Siddiqi RA, Huen IT, Handott LL,Fishman A. Perit Dial Int 23(4),368- 74 (2003)
18. Roldán M.V., Frattini A.L., Sanctis O.A., Pellegrini N.S. *Anales AFA* 17 , 212-217 (2005)
19. Panacek A, Kvitek L, Prucek R, Kolar M, Vecerova R, Pizurova N, et al. J PhysChem B 110 (33),16248-16253 (2006)
20. P.K. Sahoo , S.S. Kalyan Kamal , T. Jagadeesh Kumar, B. Sreedhar , A.K. Singh, S.K. Srivastava. Defence Science Journal 59, 447-455 (2009)
21. Shuguang Deng Pingali, K.C. Rockstraw 8,730 - 734 (2008)
22. Baker.C, Pradhan et.al. J NanosciNanotechnol 5(2):244-9 (2005)

23. Scardi, P. and Leoni, M., Acta. Cryst. A58, 190-200 (2002).

24. Warren B E, (1969). X – ray Diffraction, (Addision – Wesley, New York).

25. Somashekar R, Hall I H and Carr P D, *J ApplCryst*, 22 (1989) 363.

26. Warren B E, *Prog. Met. Phys.* 8, (1959) 147 – 202.

27. Warren B E and Averbach B L, *J. Appl. Phys*, 21 (1950) 595.

28. Veltrop L, Delhez R, De KeijserTh H, Mittemeijer E J and Reefman D, *J. Appl. Cryst*, 33 (2000) 296 – 306.